Journal of Power Sources 243 (2013) 641–647

Contents lists available at SciVerse ScienceDirect

Journal of Power Sources

journal homepage: www.elsevier.com/locate/jpowsour

Effect of cathode/anode area ratio on electrochemical performance of lithium-ion batteries

Bongki Son [a], Myung-Hyun Ryou [b], Jaecheol Choi [a], Sang-Hern Kim [a], Jang Myoun Ko [a], Yong Min Lee [a,*]

[a] Department of Applied Chemistry, Hanbat National University, Deokmyoung-dong, Yuseong-gu, Daejeon 305-719, Republic of Korea
[b] Institute of Physical Chemistry, MEET Battery Research Centre, University of Muenster, Corrensstraße 46, 48149 Muenster, Germany

HIGHLIGHTS

- Relatively larger anode causes low initial coulombic efficiency and discharge capacity.
- Rate capability and cycle life are also dependent on cathode/anode area ratio.
- Slightly larger anode area is recommended for better electrochemical properties.

ARTICLE INFO

Article history:
Received 27 March 2013
Received in revised form
9 June 2013
Accepted 10 June 2013
Available online 18 June 2013

Keywords:
Area ratio
Electrode
Rate capability
Cycle life
Electrochemical performance
Lithium-ion batteries

ABSTRACT

The effects of cathode/anode area ratio on the electrochemical performance of lithium-ion batteries are investigated using 2032-type coin full cells. As the anode area is increased from 1.13 (ø12 mm) to 2.54 cm^2 (ø18 mm) while maintaining the cathode area as 1.13 cm^2 (ø12 mm), both coulombic efficiency and discharge capacity at the first formation step become increasingly worse, probably owing to greater formation of solid electrolyte interphase (SEI). Moreover, rate capability also declined with increased anode area, whereas discharge capacity retention behavior during 1C/1C charge/discharge cycling appeared similar except for a slightly decreased capacity of coin cells with larger anode areas. The findings indicate that cathode/anode area ratio should be carefully evaluated to achieve reliable data on electrochemical performance.

1. Introduction

Lithium-ion batteries (LIBs) lead the secondary battery market and are regarded as the most promising large-format secondary battery for electric vehicles (EVs) and energy storage systems (ESSs) [1–3]. As a result, this technology has recently attracted much greater attention from the academic and industrial research communities. Some studies have reported deficient electrochemical properties, which we attribute to a lack of information on electrode or cell design parameters and improper experimental conditions, because such factors can sometimes have more significant effects on electrochemical properties than materials themselves [4,5]. Among various design parameters, the issue of compositional changes in the electrode has attracted the most attention, owing to ease of application [6,7]. In comparison, a few research groups have examined other important parameters such as electrode thickness and density [4,5,8–12], but their results are not sufficiently varied to permit extrapolation to differing electrode systems. Another important factor is the capacity ratio of negative electrode (anode) to positive electrode (cathode). This so-called N/P ratio has not been well explored to provide useful information for LIBs [13,14]. Furthermore, the cathode/anode area ratio has not been a research topic for LIBs, to our knowledge, even though it can affect electrochemical properties such as rate capability and cycle performance.

In this work, we prepared five types of coin full cells with different cathode/anode area ratios, as shown in Fig. 1 and Table 1. The initial coulombic efficiencies and discharge capacities were precisely monitored while all the cells were cycled during one formation cycle and three subsequent stabilization cycles, which

* Corresponding author. Tel.: +82 42 821 1549; fax: +82 42 821 1692.
E-mail address: yongmin.lee@hanbat.ac.kr (Y.M. Lee).

0378-7753/$ – see front matter © 2013 Elsevier B.V. All rights reserved.
http://dx.doi.org/10.1016/j.jpowsour.2013.06.062

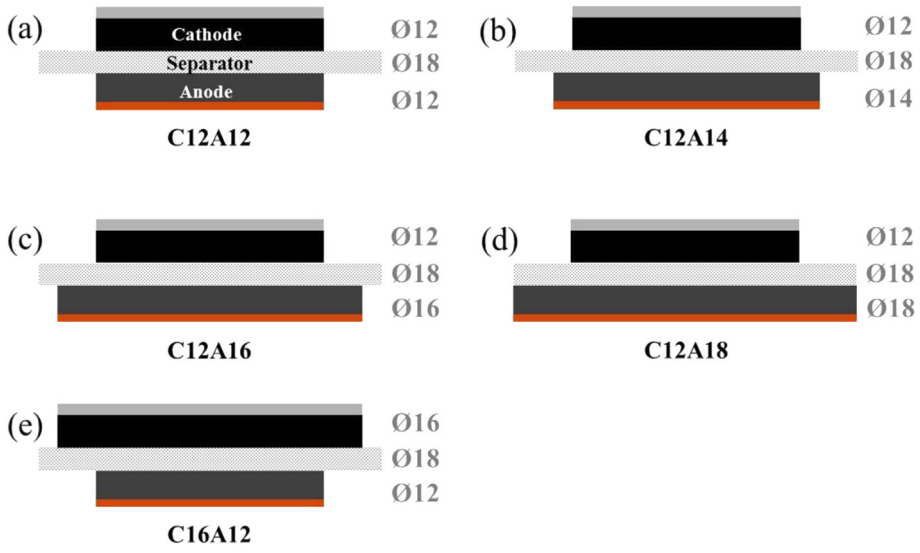

Fig. 1. Schematic diagrams of five types of coin cells with different cathode/anode area ratios.

are defined by precycling. Their rate capability and cycle performance were then evaluated via electrochemical impedance spectroscopy.

2. Experimental

2.1. Preparation of cathodes and anodes

Cathodes were prepared by coating N-methyl-2-pyrrolidone-based slurry (NMP, Sigma–Aldrich, USA) consisting of 92 wt.% $LiCoO_2$ (10 μm, KD-10, Umicore Korea, Korea), 4 wt.% conductive carbon (Super-P, Timcal, Switzerland), and 4 wt.% polyvinylidene fluoride (PVdF, Solef-6020, Solvay Chemicals, Belgium) binder onto Al current collector foil (15 μm, Sam-A Aluminium, Korea). The active material loading level of cathodes in this work was 11.8 mg cm^{-2}. The cathode thickness and density were controlled to be 42 μm and 2.80 g cm^{-3}, respectively.

Anodes were prepared similarly, by coating NMP-based slurry consisting of 93 wt.% artificial graphite (20 μm, SCMG-AR, Showa Denko, Japan), 2 wt.% Super-P, and 5 wt.% PVdF binder onto Cu current collector foil (10 μm, Nippon Foil, Japan). The active material loading level of anodes in this work was 6.1 mg cm^{-2}. The anode thickness and density were 37 μm and 1.65 g cm^{-3}, respectively. Information on the cathode and anode is summarized in Table 2.

The surface and cross-sectional morphologies of the cathode and anode were characterized by normal scanning electron microscope (SEM, JSM-6390, JEOL, Japan) and field emission scanning electron microscope (FE-SEM, S4800, Hitachi, Japan), respectively. In order to prepare a cross-sectional specimen of each cathode, it was cut by an argon-ion beam polisher (E3500, Hitachi) at a constant power of 2.1 W (6 kV and 0.35 mA) under vacuum ($<2.0 \times 10^{-4}$ Pa).

Table 1
Dimensional information for each cathode and anode.

ID	CA diameter (Ø, mm)	AN diameter (Ø, mm)	CA area (cm^2)	AN area (cm^2)	Area ratio (AN/CA)
C12A12	12	12	1.13	1.13	1.00
C12A14	12	14	1.13	1.54	1.36
C12A16	12	16	1.13	2.01	1.78
C12A18	12	18	1.13	2.54	2.25
C16A12	16	12	2.01	1.13	0.56

2.2. Cell assembly

Each cathode and anode was punched to a disc of designed diameters, shown in Table 1. While maintaining the cathode area as 1.13 cm^2 (ø12 mm), the anode areas were 1.13 (ø12 mm), 1.54 (ø14 mm), 2.01 (ø16 mm) and 2.54 cm^2 (ø18 mm). In addition, the opposite case study was performed, with a cathode of 2.01 cm^2 (ø16 mm) and anode of 1.13 (ø12 mm). After the punching process, electrodes were dried at 80 °C for 12 h under vacuum. The corresponding cathode and anode were assembled to 2032-type coin full cells with polyethylene (PE) separators (thickness: 20 μm, area: ø18 mm, ND420, Asahi Kasei E-materials, Japan) and 1.15 M $LiPF_6$ in ethylene carbonate (EC)/ethylmethyl carbonate (EMC) (3/7, by volume, PANAX ETEC, Korea) as an electrolyte. All the cell assembly and disassembly processes were performed in an argon-filled glove box, in which the dew point was maintained at less than −80 °C.

2.3. Electrochemical testing

After assembly, the unit cells were aged for 12 h, and then cycled between 3.0 and 4.2 V at a constant current (CC) of 0.1C rate in both

Table 2
Materials, compositions, loading levels, thicknesses, densities, porosities, and designed capacities of the prepared cathode and anode.

	Unit	Cathode	Anode
Active material (AM)	–	$LiCoO_2$ (KD-10, Umicore)	Artificial graphite (SCMG-AR, Showa Denko)
Specific capacity	mAh g^{-1}	140	360
Conductor	–	Super-P (Timcal)	
Binder	–	Polyvinylidene fluoride (Solef-6020, Solvay Chemicals)	
Composition (AM: Conductor:Binder)	wt.%	92:4:4	93:2:5
Loading level	mg cm^{-2}	11.8	6.1
Electrode thickness	μm	42	37
Electrode density	g cm^{-3}	2.80	1.65
Electrode porosity	%	37.3	20.7
Nominal capacity	mAh cm^{-2}	1.50	1.70

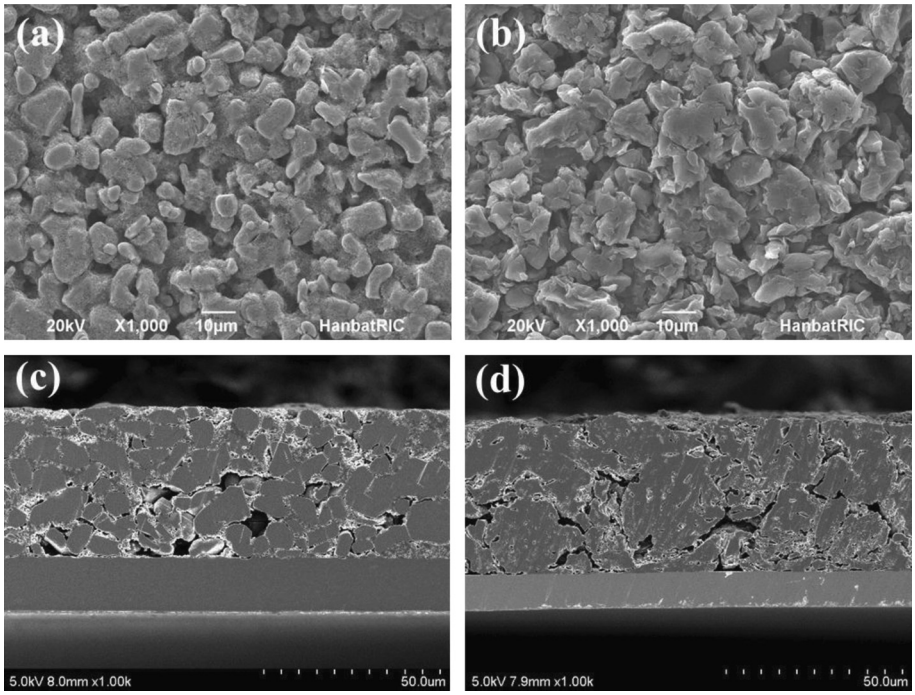

Fig. 2. SEM images of (a) cathode surface, (b) anode surface, (c) cathode cross-section, and (d) anode cross-section.

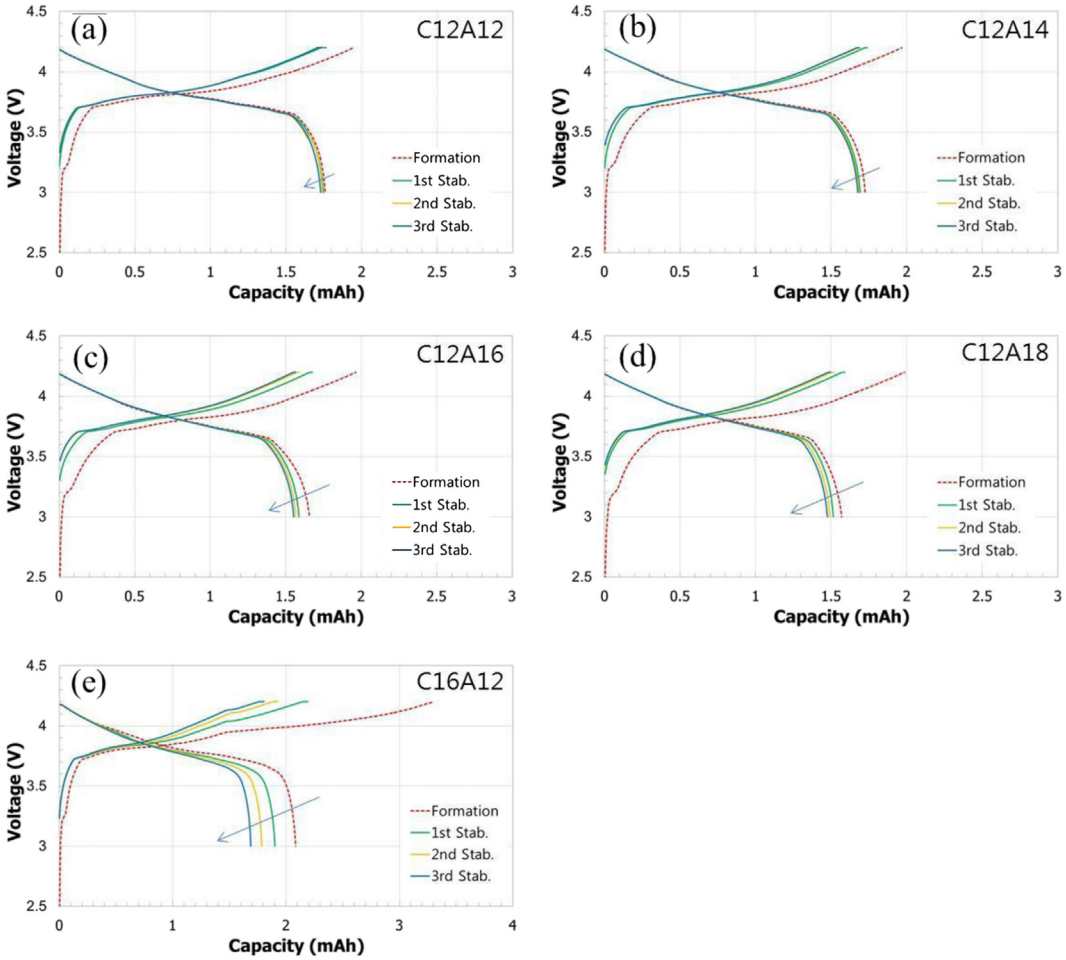

Fig. 3. Voltage profiles of coin cells with different cathode/anode area ratios [(a) C12A12, (b) C12A14, (c) C12A16, (d) C12A18, and (e) C16A12] during precycling.

charging and discharging processes as a formation step, using a charge/discharge cycler (PNE Solutions, Korea) at 25 °C. In order to stabilize the corresponding unit cells, they were cycled between 3.0 and 4.2 V at a slightly higher current density of 0.2C for an additional 3 cycles. The rate capability of unit cells was evaluated by increasing discharging current densities from 1 to 5C (1, 2, 3, and 5C) in a CC mode while maintaining the charging current density of 1C in a constant current/constant voltage (CC/CV) mode. Each c-rate was repeated for 10 cycles. Each unit cell was also cycled at a current density (1C rate, CC in discharge, and CC/CV at charge between 3.0 and 4.2 V) for 100 cycles at 25 °C. The electrochemical impedance of the unit cells after precycling and cycle tests was obtained via a VSP impedance analyzer (Bio-logic SAS, France) over a frequency range of 0.04 Hz to 1 MHz at an amplitude of 10 mV.

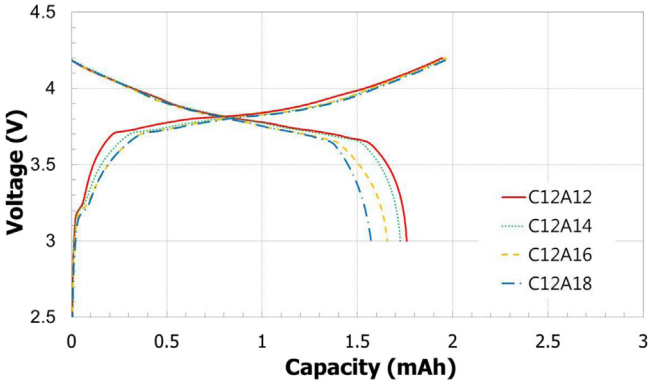

Fig. 4. Voltage profiles of four coin cells with different cathode/anode area ratios during the formation step.

3. Results and discussion

As shown in Fig. 1 and summarized in Table 1, five types of coin full cells were prepared with different cathode/anode area ratios. As shown in Fig. 1(a–d), the anode area was larger than the cathode, in order to prevent the formation of lithium dendrite on the anode, and to ensure that both cathode and anode were well aligned. For the opposite case study, the cathode of 2.01 cm^2 (ø16 mm) was paired with the smaller anode of 1.13 cm^2 (ø12 mm). Each coin cell was denoted as "CxxAyy," where Cxx and Ayy indicate the cathode and anode diameters, respectively. For example, C12A18 indicated a coin cell comprising a ø12-mm $LiCoO_2$ cathode and ø18-mm artificial graphite anode.

The composition, loading level, electrode thickness, and the density, porosity and nominal capacity of the cathode and anode are as summarized in Table 2. The cathode and anode parameters in this work were thought to be appropriately designed within the range of electrode design parameters for commercial applications such as mobile IT, hybrid EVs, and ESSs [4]. From the nominal capacity data, the N/P ratio was calculated to be about 1.13, which was also comparable to conventional LIBs.

The surface and cross-sectional morphologies of the cathode and anode are shown in Fig. 2. They seemed to be well manufactured to give homogeneous dispersion and appropriate porosities of 37.3% for cathode and 20.7% for anode, respectively, which were calculated from the true density of each electrode component and electrode physical properties [4].

Fig. 3 shows the voltage profiles of manufactured coin cells during precycling, comprising of one formation cycle and three subsequent stabilization cycles. The cells' charged and discharged capacities, and their coulombic efficiencies during precycling are also summarized in Table 3. As the anode area was gradually increased from 1.13 to 2.54 cm^2, first the initial coulombic efficiency shows a large drop from about 90% to 79% owing to increased SEI formation reaction on the anode. As shown in Fig. 4, which was redrawn for the formation step only, the coin cells with larger anodes show increased decomposition reaction at the beginning of charging process and decreased discharge capacity. The former could be confirmed by slower increase in voltage to a plateau starting around 3.7 V, as reported in previous studies [15,16]. Although the charged capacity was also increased by approximately 2% (from 1.945 to 1.987 mAh) with larger anode areas (see Table 3), the discharge capacity showed a much greater reduction of approximately 11%, from 1.759 (C12A12) to 1.571 mAh (C12A18), which implies that some of lithium ions during charging were irreversibly consumed to form SEI, not to be intercalated into a graphite anode.

Another interesting point was the capacity stabilization behavior during the precycling, as shown in Fig. 3 and Table 3. Whereas the C12A12 coin cell maintained its discharge capacity at the initial value with quickly saturated coulombic efficiency, C12A18 showed continuous capacity decrease and lower stabilization rate. Moreover, the charging voltage plateau showed larger gaps between the formation and stabilization step as the anode area increases. On the other hand, there was no difference in the discharging voltage plateau, which means that the charging process was more resistive than the discharging process.

In order to investigate the opposite case, in which the cathode area was larger than the anode, the C16A12 coin cell was also evaluated and presented in Fig. 3(e) and Table 3. Although the charged capacity during the formation step seems to reach the theoretical value, the discharge capacity was greatly reduced to give a very low coulombic efficiency of around 63%. Moreover, the discharge capacity showed a much greater continuous decrease with relatively low coulombic efficiencies during the stabilization cycles. We thought that this different phenomenon was closely related to irreversible lithium dendrite formation on both anode surface and coin cell bottom. As shown in Fig. 5(a), metallic lithium dendrite was easily found near the edge of the anode on the coin

Table 3
Charge/discharge capacities and coulombic efficiencies of coin cells with different cathode/anode area ratios [(a) C12A12, (b) C12A14, (c) C12A16, (d) C12A18, and (e) C16A12] during precycling comprising one formation cycle and three stabilization cycles.

	Formation			1st stab.			2nd stab.			3rd stab.		
	CHG (mAh)	DIS (mAh)	Coul. eff. (%)	CHG (mAh)	DIS (mAh)	Coul. eff. (%)	CHG (mAh)	DIS (mAh)	Coul. eff. (%)	CHG (mAh)	DIS (mAh)	Coul. eff. (%)
C12A12	1.945	1.759	**90.4**	1.765	1.747	99.0	1.743	1.741	99.9	1.739	**1.729**	99.4
C12A14	1.968	1.725	**87.7**	1.738	1.693	97.4	1.696	1.683	99.2	1.685	**1.677**	99.5
C12A16	1.965	1.656	**84.3**	1.677	1.587	94.6	1.590	1.566	98.5	1.566	**1.552**	99.1
C12A18	1.987	1.571	**79.1**	1.592	1.515	95.2	1.521	1.492	98.1	1.497	**1.476**	98.6
C16A12	3.297	2.085	**63.2**	2.191	1.902	86.8	1.931	1.786	92.5	1.805	**1.689**	93.6

The two properties (columbic efficiencies in the formation and discharge capacities tin the 3rd stabilization) are in bold due to significant differences among the samples.

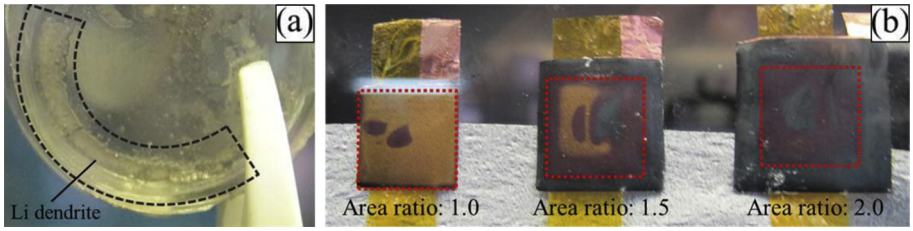

Fig. 5. Digital camera images of (a) metallic lithium dendrite on the coin cell bottom, and (b) fully charged graphite anodes disassembled from the pouch-type cells (dotted line indicates the faced area with $LiCoO_2$ cathodes).

cell bottom after c-rate and cycle tests. Therefore, this obvious result might explain why the anode area should be greater than or equal to that of the cathode.

Meanwhile, since the color of the anode was readily changeable according to the state-of-the-charge (SOC), three pouch-type cells with different cathode/anode area ratios (1/1, 1/1.5 and 1/2, in a rectangular type) were also manufactured. After all the cells were precycled, they were fully charged and disassembled in the glove box. At an area ratio of 1/1, most of the anode region showed yellowish color, indicating that all the graphene layers were fully filled with lithium ions [17], except for a few small dark spots. However, as the anode area became increasingly larger than the cathode, the yellowish area gradually decreases owing to the intercalation of lithium ion into the outer anode region, which did not overlie the cathode. In the case of an area ratio of 1/2, there was no yellowish region on the anode; in other words, lithium ions could freely move to any region of the anode.

The effects of cathode/anode area ratios on electrochemical properties were investigated through rate capability and cycling tests. First, the voltage profiles at different c-rates are shown in Fig. 6. As the anode area increases, discharge capacity retention deteriorates. Since the charge current was fixed to 1C for all cells, which implied that almost the same number of lithium ions was well intercalated into the anode irrespective of its area, this difference may be mainly related to local SOCs of the graphite anodes overlaid with cathodes. As confirmed by Fig 5(b), the local SOC of the fully charged anode was inversely proportional to its area. Therefore, unit cells with smaller anodes showed greater electrochemical reactivity, thereby resulting in better rate capability properties. Furthermore, since the lithium ions that were intercalated into the outer anode region are subject to

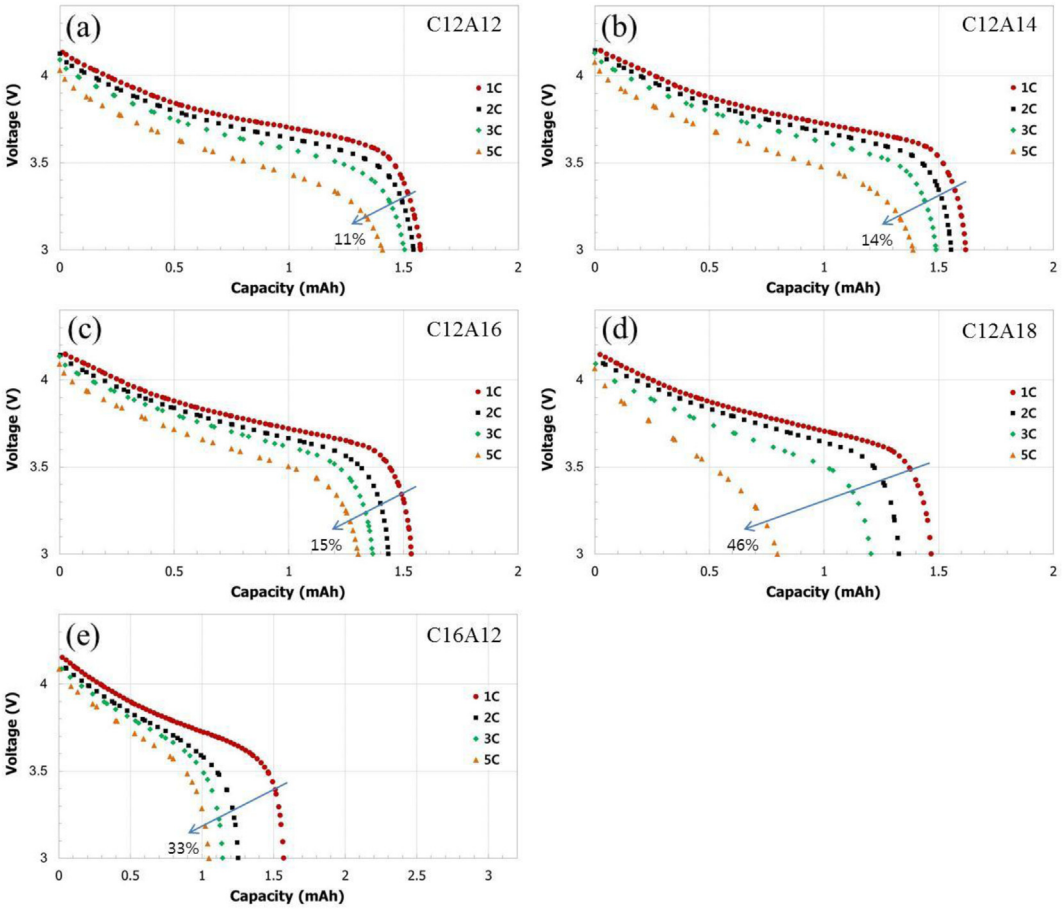

Fig. 6. Discharge curves at various c-rates for coin cells with different cathode/anode area ratios [(a) C12A12, (b) C12A14, (c) C12A16, (d) C12A18, and (e) C16A12].

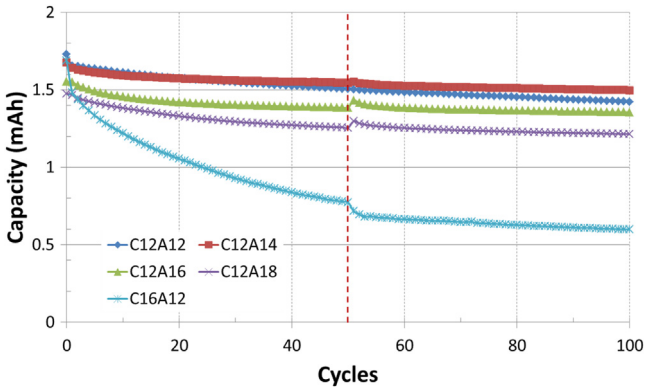

Fig. 7. Capacity retention of coin cells with different cathode/anode area ratios [(a) C12A12, (b) C12A14, (c) C12A16, (d) C12A18, and (e) C16A12] as a function of cycle number (vertical dotted line means the specific cycle number at which cycling stops for a while and continues).

weaker electrical field and must move longer distance from anode to cathode, the rate capability was lower. In case of the C16A12 cell, although it seemed to have similar discharge capacities to the other cells, its discharge capacity was less than half, considering the cathode area was approximately doubled.

The 1C/1C cycle life of each unit cell was also evaluated, and the results are presented in Fig. 7. Except for the opposite case (cell C16A12), the other four cases showed very stable capacity retention behavior for 100 cycles, even though the absolute capacity of unit cells with larger anodes was slightly low. However, the C12A12 cell showed slightly more rapid capacity fading, starting around the 30th cycle. This could be explained by insufficient anode capacity, some of which might contribute to irreversible SEI formation and continuous electrolyte decomposition during cycling, although the N/P ratio was designed to be 1.13. In order to verify these, we measured XPS analysis on central area of anode overlapped with cathode and oversized extra area without overlapping with cathode. As shown in Fig. 8, both cases demonstrated almost similar XPS profiles for C 1s, O 1s, F 1s, and P 2p. This suggests that SEI is uniformly formed on both areas as we suggested above. Meanwhile, the C16A12 cell showed the worst capacity retention behavior, which was probably because of the persistent formation of lithium dendrite and electrolyte decomposition. Therefore, this result suggested that the anode capacity should be greater than the cathode via control of N/P or area ratio. However, since higher capacity for an anode with the same active materials could only be achieved by increasing the electrode

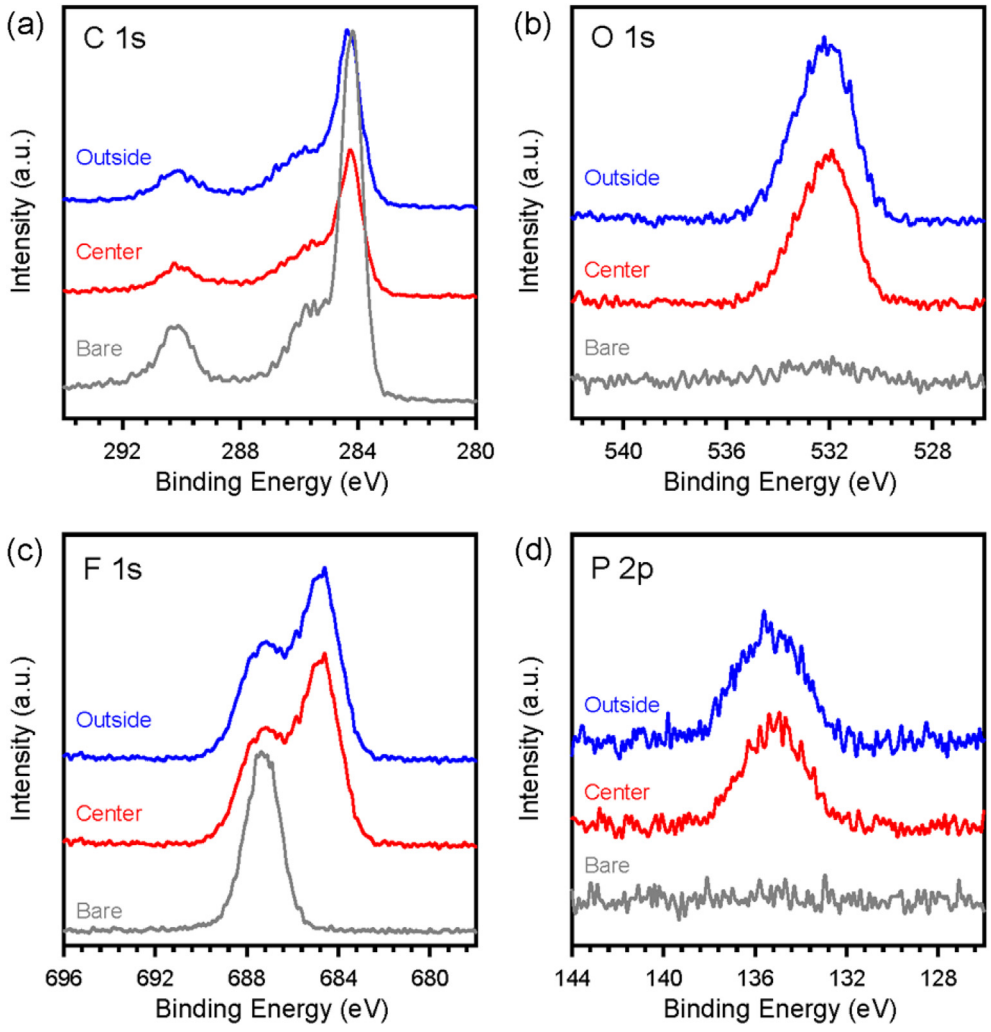

Fig. 8. XPS profiles of (a) C 1s, (b) O 1s, (c) F 1s, and (d) P 2p on bare anode and precycled anode (center point in the overlapped area and outside point in the oversized extra area).

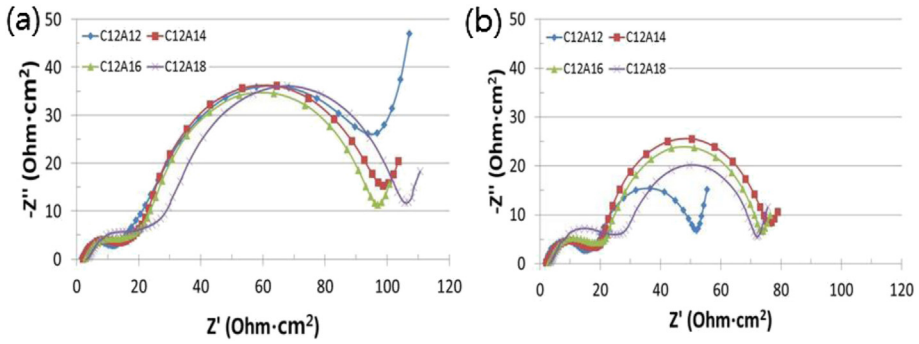

Fig. 9. EIS results of coin cells with different cathode/anode area ratios (a) after precycling and (b) after cycle performance (1C, 100 cycles).

thickness or density, management of the N/P ratio could be applied in some limited cases [4].

In order to evaluate the effects of cathode/anode area ratio on the resistance of the cells, electrochemical impedance spectroscopy measurements were conducted after precycling and cycle performance (1C-rate, 100 cycles). Unfortunately, however, we could not bring a reasonable implication out of EIS results as shown in Fig. 9. Among various reasons making EIS analysis difficult, in our system, the inhomogeneity of state of charge in oversized electrode seems to be a main reason. As discussed above, outside electrode area not overlapped with counter electrode inherently has the different state of charge compared to that of central area, overlapped area with counter electrode. Considering the facts that EIS profiles including a size and a pattern are largely dependent on the state of charge for both cases of anode and cathode, respectively [18,19], in conclusion, it is impossible to make a reliable implication from the EIS results out of our experimental cases. Even worse, there is no technique to distinguish each area at present.

Although this work was conducted using a laboratory-scale coin cell system, the results were meaningful and could be reliable for many forms of battery research. Therefore, the findings provided a good reference to consider and select appropriate electrode pairs.

4. Conclusion

The cathode/anode area ratio is an important factor in achieving different electrochemical properties with the same electrodes. As the anode area increases, not only the coulombic efficiency and discharge capacity during precycling but also rate capability and cycle life are also largely degraded due to increased SEI formation reaction and low local SOC level on the anode. However, since electrochemical impedance spectroscopy is found to be more dependent on the electrode area, it cannot provide reliable experimental results to explain the corresponding electrochemical properties. However, it is recommended that anode area should be at least slightly larger than the cathode for longer cycle life under the commercial cell-level N/P ratio.

Acknowledegement

This research was financially supported by the Ministry of Education, Science, and Technology (MEST) and by the National Research Foundation of Korea (NRF) through the Human Resource Training Project for Regional Innovation and General Researcher Project (2010-0025738).

References

[1] K. Kang, Y.S. Meng, J. Bréger, C.P. Grey, G. Ceder, Science 311 (2006) 977.
[2] A.L.M. Reddy, S. Nagarajan, P. Chumyim, S.R. Gowda, P. Pradhan, S.R. Jadhav, M. Dubey, G. John, P.M. Ajayan, Sci. Rep. 2 (2012) 960.
[3] B. Dunn, H. Kamath, J.-M. Tarascon, Science 334 (2011) 928.
[4] J. Choi, B. Son, M.-H. Ryou, S.H. Kim, J.M. Ko, Y.M. Lee, J. Electrochem. Sci. Technol. 4 (1) (2013) 27.
[5] Y.-H. Chen, C.-W. Wang, X. Zhang, A.M. Sastry, J. Power Sources 195 (2010) 2851.
[6] J. Li, C. Daniel, D. Wood, J. Power Sources 196 (2011) 2452.
[7] C. Fongy, A.-C. Gaillot, S. Jouanneau, D. Guyomard, B. Lestriez, J. Electrochem. Soc. 157 (2010) A885.
[8] J. Shim, K.A. Striebel, J. Power Sources 119–121 (2003) 934.
[9] J. Shim, K.A. Striebel, J. Power Sources 130 (2004) 247.
[10] V. Srinivasan, J. Newman, J. Electrochem. Soc. 151 (2004) A1530.
[11] H. Zheng, J. Li, X. Song, G. Liu, V.S. Battaglia, Electrochim. Acta 71 (2012) 258.
[12] S. Yu, Y. Chung, M.S. Song, J.H. Nam, W.I. Cho, J. Appl. Electrochem. 42 (2012) 443.
[13] R. Xue, H. Huang, G. Li, L. Chen, J. Power Sources 55 (1995) 111.
[14] N. Gunawardhana, G.-J. Park, A.K. Thapa, N. Dimov, M. Sasidharan, H. Nakamura, M. Yoshio, J. Power Sources 203 (2012) 257.
[15] M. Winter, P. Novák, A. Monnier, J. Electrochem. Soc. 145 (1998) 428.
[16] F. Joho, B. Rykart, A. Blome, P. Novák, H. Wilhelm, M.E. Spahr, J. Power Sources 97–98 (2001) 78.
[17] G. Park, N. Gunawardhana, H. Nakamura, Y. Lee, M. Yoshio, J. Power Sources 196 (2011) 9820.
[18] J. Hong, C. Wang, U. Kasavajjula, J. Power Sources 162 (2006) 1289.
[19] S.S. Zhang, K. Xu, T.R. Jow, Electrochim. Acta 51 (2006) 1636.